J Mater Sci (2018) 53:12795–12806

Chemical routes to materials

One-step mechanochemical synthesis of plasmonic Ag/Zn–Al LDH with excellent photocatalytic activity

Zhao Li[1], Qiwu Zhang[1,2,*], Xinzhong Liu[3], Lei Wu[1], Huimin Hu[1], and Yue Zhao[1]

[1] School of Resources and Environmental Engineering, Wuhan University of Technology, Wuhan 430070, China
[2] Hubei Key Laboratory of Mineral Resources Processing and Environment, Wuhan University of Technology, Wuhan 430070, China
[3] College of Ecological Environment and Urban Construction, Fujian University of Technology, Fuzhou 350118, China

Received: 19 April 2018
Accepted: 31 May 2018
Published online: 6 June 2018

ABSTRACT

A series of Ag/Zn–Al layered double hydroxide composites were successfully synthesized by a mechanochemical method, and their photocatalytic activity as methyl orange (MO) degradation was investigated. The nanoscale composites showed excellent photocatalytic activity and enabled simply over 95% degradation of MO under visible light irradiation in 180 min. Based on the results from EIS and PL analyses, the enhancement of photocatalytic efficiency was mainly attributed to the surface plasmon resonance effect of Ag nanoparticles and the Schottky barrier between Ag and LDH, with efficient adsorption of resonant photons on the composites and subsequent electron transfer to the conduction band of LDH to promote the separation efficiency of photogenerated electrons and holes. 4%Ag/LDH exhibited the highest photocatalytic activity with high stability after multiple running cycles. The electron spin resonance revealed that ·OH was the dominant active species in the photocatalysis process. Considering the limited choice of soluble noble metal salts to serve as starting samples for loading preparation, this work allowed the direct use of Ag metal instead of very expensive soluble salts for sample preparation, providing a facile novel green and nonthermal method to assemble metal–semiconductor combination by co-grinding metal element with semiconductor raw materials.

Introduction

As humankind is facing increasingly serious environmental pollution and energy shortage [1–3], semiconductor photocatalysis technology has received widespread attention [4–7]. Among all reported semiconductor photocatalysts, layered double hydroxides (LDHs) were considered as a promising candidate to replace TiO_2. LDHs known as anionic or hydrotalcite-like clays possess a general formula $\left[M^{2+}_{1-x}M^{3+}_{x}(OH)_2\right]^{X+}\left[A_{x/n}\right]^{n-}\cdot mH_2O$, where M^{2+}, M^{3+} and A^{n-} are divalent, trivalent metal cations and interlayer anion, respectively [8]. LDHs exhibit two major structural advantages as photocatalysts. Firstly, the host layers of LDHs provide

Address correspondence to E-mail: zhangqw@whut.edu.cn

https://doi.org/10.1007/s10853-018-2537-4

abundant basic loading sites, enabling their application as heterogeneous solid base catalysts. Moreover, the uniform distribution of two or more photoactive metal cations on LDH layers at the atomic level avoids the screens between separate cations, providing expected photocatalytic activity and even selectivity [9–11].

Among all the reported LDH photocatalytic materials [12–15], Zn–Al LDHs were considered highly capable of degrading organic pollutants due to the significant adsorption and photocatalysis synergism [16–18]. However, LDHs exhibit two serious limitations of practical application: the rapid recombination of charge carriers [19] and the confined UV light response capability [8]. Therefore, further researches should be focused on promoting the separation of photogenerated charge carriers and increasing the utilization of solar light.

At present, plasmonic noble metals have been intensively studied for loading on semiconductors due to its unique characteristics [20–22]. After combining with semiconductors, the collective oscillations with a resonant frequency of conduction electrons can be induced by noble metals due to the strong surface plasmon resonance (SPR), which may enhance the absorption of visible light [23–26]. Simultaneously, the photogenerated electrons can be transferred between noble metal and conduction band of semiconductor which act as electron trappers due to the Schottky barriers formed at metal–semiconductor interface, while the holes can remain on the valence band [27, 28]. This combination can prompt the detachment of photogenerated electrons from the excitation site of both semiconductors and metals and prevent the recombination of charge carriers to provide a better opportunity for their consumption in photodegradation. Of all noble metals, silver is favored because of its relatively low price and hypotoxicity [29]. Hence, hybridizing Ag with Zn–Al LDH in an appropriate method may boost bulk charge separation and enhance visible light utilization of Zn–Al LDH. However, the traditional methods to manufacture noble metal–semiconductor composites involve the reduction in soluble salt of noble metal, of which Ag nitrate is one choice, by organic reducing agents such as hydrazine hydrate. The toxicity of noble metal soluble salts and the secondary pollution risk of liquid phase reaction require strongly the development of a facile and green method to prepare the metal–semiconductor combination. Several studies have shown that $AgNO_3$ can be reduced to Ag by mechanochemical methods [30, 31]. Beyond this, it is reasonable to carry out the research of directly loading available element Ag on LDH through mechanochemical procedure.

In this work, we report the design of Ag/Zn–Al LDH through co-grinding of elemental silver and raw materials for LDH. The as-synthesized Ag/LDH photocatalysts displayed remarkably enhanced photocatalytic activity toward the degradation of dye-contained sewage under visible light irradiation, as compared with that of mechanochemically synthesized pure Zn–Al LDH. The composite structures were characterized, and the SPR effect originated from the mechanochemically induced interaction between elemental silver and LDH was found to efficiently enhance the photocatalytic performance. The mechanism of improving photocatalytic capacity along with its reusability has been addressed and thoroughly discussed with the obtained structure.

Experimental procedure

Reagents and materials

Zinc carbonate hydroxide hydrate ($Zn_4CO_3(OH)_6{\cdot}H_2O$), aluminum hydroxide ($Al(OH)_3$), elemental silver (Ag) and methyl orange (MO) were purchased from Sinopharm Group Co Ltd., Shanghai, China, Analytical reagent. All chemicals were used without further purification. All solutions were prepared with analytical grade reagents and high purity deionized water produced by a Milli-Q® system (Millipore, Bedford, MA, USA).

Mechanochemical synthesis of Ag/LDH nanostructures

A planetary ball mill (Pulverisette-7, Fritsch, Germany), which has two mill pots (45 cm^3 inner volume each) made of zirconium dioxide with 7 zirconium dioxide balls of 15 mm in diameter, was used to conduct the ball-milling operation. The milling intensity was fixed at 600 rpm for 2 h.

Pure Zn–Al LDH was synthesized by a mechanochemical operation. In the first dry grinding process, 2 g of zinc carbonate hydroxide hydrate and $Al(OH)_3$ (Zn/Al molar ratio fixed at 2/1) mixture were ground to obtain the LDH precursor. In the

second agitation step, 1 g of the precursor was put into a capped erlenmeyer flask filled with 100 mL of water and stirred for 4 h on the magnetic stirring apparatus (524G, Meiyingpu, Shanghai, China) at 1200 rpm.

Ag/LDH composites were synthesized by grinding 2 g of zinc carbonate hydroxide hydrate, $Al(OH)_3$ and elemental silver. The amount of Ag was adjusted to be 1, 2, 3, 4 and 5% to LDH in weight ratio. After grinding, the precursor was water stirred and dried as above described. The preparation procedure is schematically illustrated in Fig. 1.

Characterizations

Phase compositions and crystal structures of the as-synthesized samples were identified by X-ray diffraction (XRD) using a Rigaku Max-RB RU-200B diffractometer using CuKα radiation (λ = 1.5403 Å) at 2θ between 5° and 70°. A UV/VIS/NIR Spectrometer (Lambda 750 S, PerkinElmer) was used to record the UV–Vis spectra of the prepared samples. A SEM (JSM-5610LVJEOL) spectroscopic measurement with EDS accessory (Phoenix, EDAX) was used to observe the microstructures and the distribution of Ag on LDH matrix of the as-prepared composites. X-ray photoelectron spectroscopy (XPS) was performed on an ESCALAB 250Xi system. Electrochemical impendence spectroscopy (EIS) was measured in a 1 M Na_2SO_4 solution with sinusoidal ac perturbation of 5 mV over a frequency range from 0.1 to 100000 Hz, on an electrochemical workstation VersaSTAT 4, AMETEK. The photoluminescence (PL) spectra were collected at room temperature using F-380 FL spectrophotometer, GANGDONG with a 150 W xenon lamp as an excitation source at 325 nm excitation wavelength. ESR spectra for hydroxyl radicals (·OH) and superoxide radicals ($\cdot O^{2-}$) were measured by a BRUKER A300 spectrometer (Germany) at 3450 G and 9.818 GHz. Before recording, 10 mg sample was dissolved in 0.5 mL deionized water or methanol, and then 30 μL of 5,5-dimethyl-1-pyrroline N-oxide (DMPO) was added with ultrasonic dispersion for 5 min, respectively.

Photocatalytic activity test

The photocatalytic activities of pure Zn–Al LDH and Ag/LDH composites were evaluated by the degradation of MO with a concentration of 100 mg/L. 0.16 g of photocatalytic was added into 200 mL solution in a quartz breaker. The mixture was first kept in dark for 1 h under magnetic stirring to ensure the adsorption equilibrium. Afterward, a 500 W Xenon lamp (PLS-SXE300, Perfect Light) was used as a UV–Vis light source ($\lambda \geq 420$ nm). After certain intervals, 4 mL of the treated solution was extracted and centrifuged, followed by the measurement of remaining MO concentration in the supernatant on a SHIMADZU UVmini-1240 UV/VIS spectrometer at 463 nm. The blind reaction was also carried out by the same procedure without adding any catalysts.

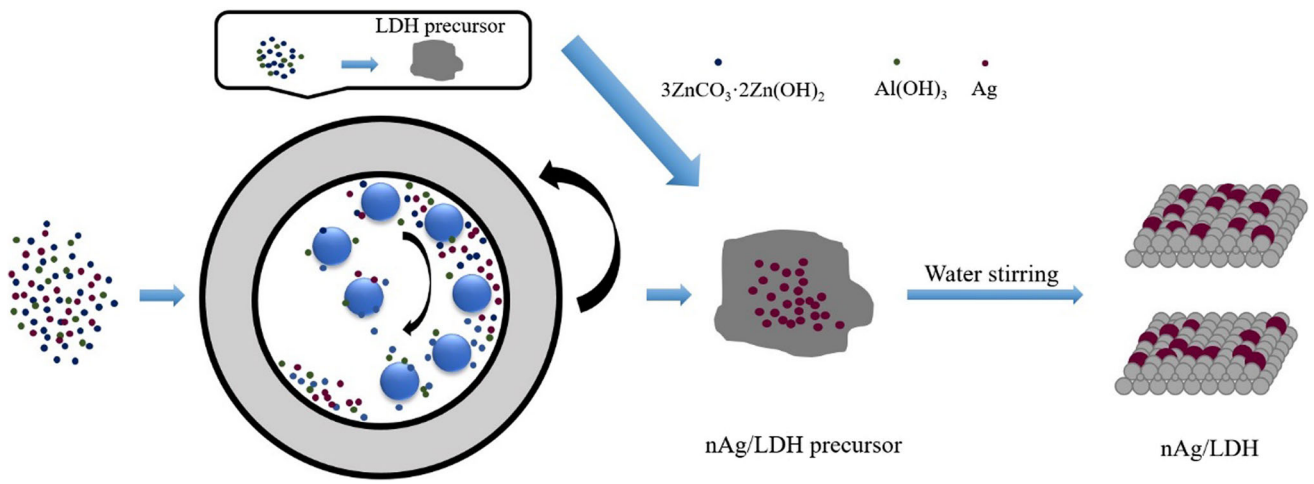

Figure 1 Schematic illustration of the synthesis procedure of *n*Ag/Zn–Al LDH as photocatalysts by a ball-milling approach.

Results and discussion

Structure characterization

XRD patterns of Zn–Al LDH and Ag/LDH are shown in Fig. 1. The reflections of LDH, such as (003), (006), (012), (015), (018), (110) and (113), were coincidently indexed to typical LDH (JCPDF 48-1023) as we previously reported [32–35]. No obvious changes of reflections were noted with increasing Ag content, which indicated that the mechanochemical loading of Ag did not affect the crystal of structure of LDH. At the same, the characteristic reflections of Ag (38.1°, 44.4° and 64.5°), corresponding to the cubic Ag (JCPDF 04-0783), were observed in the Ag/LDH composites. No evidence for the incorporation of Ag into the structure of LDH was observed, due to the very stable state of the used element Ag, as well as other barriers of larger Ag^{+} (1.26 Å) ions to substitute the relatively smaller Zn^{2+} (0.74 Å) and Al^{3+} (0.52 Å). The synthesis reaction could be expressed as follows (Fig. 2):

$$\mathrm{Ag} + \mathrm{Zn_4CO_3(OH)_6{\cdot}H_2O} + \mathrm{Al(OH)_3} \rightarrow \mathrm{Ag} + \mathrm{Zn_{0.67}Al_{0.33}(OH)_2(CO_3)_{0.165}{\cdot}H_2O} \quad (1)$$

XPS analyses were conducted to further identify the surface composition and chemical state of Ag/LDH assembled architectures (Fig. 3). The survey spectra (Fig. 3a) showed the full spectra of the sample, which proved the existences of Zn, Al, C, O, H and Ag elements on the surface of the Ag/LDH composite. The elements with close connection to the photocatalysis of the sample were chosen for detailed high-resolution analyses. Figure 3b exhibits the high-resolution spectra of Zn 2*p* state, with doublet peaks at 1020.78 and 1043.88 eV associated with the binding energy of Zn $2p_{3/2}$ and Zn $2p_{1/2}$, respectively, implying that Zn existed in a divalent oxidation state in LDH [36, 37]. As shown in Fig. 3c, the O 1*s* signals of pure LDH and 4%Ag/LDH could be divided into two peaks. The binding energy of 531.80 and 531.64 eV can be attributed to the hydroxyl form (OH-group) for pure LDH and 4%Ag/LDH, respectively. The other binding energy of 532.10 and 531.94 eV might be attributed to the adsorbed water (H_2O) [38, 39]. Figure 3d presents the binding energies of Ag $3d_{5/2}$ and Ag $3d_{3/2}$ located at 367.84 and 373. 84 eV, respectively, with splitting of 6 eV. Compared with traditional bulk Ag with spectra located at about 368.2 and 374.2 eV [40], the peak shift of Ag/LDH slightly to lower binding energy could be attributed to the electron transfer between Ag and LDH matrix. All the position changes in binding peaks of Zn 2*p*, O 1*s* and Ag 3*d* between the pure LDH and Ag/LDH indicated the existence of chemical interaction between Ag and LDH, rather than a simple physical mixing state. The interaction would result in the adjustment of the position of corresponding Fermi energy of Ag and LDH to a new balance after the attachment. The free electrons would transfer from Ag to the conduction band of LDH. The Schottky barrier formed at metal–semiconductor interface between Ag and LDH could promote the separation of charges and prevent the recombination [21, 28, 37]. Ultimately, the potential of Ag Fermi level became more positive and the Ag electron density was also decreased, after the combining with LDH and the resulting electron transference.

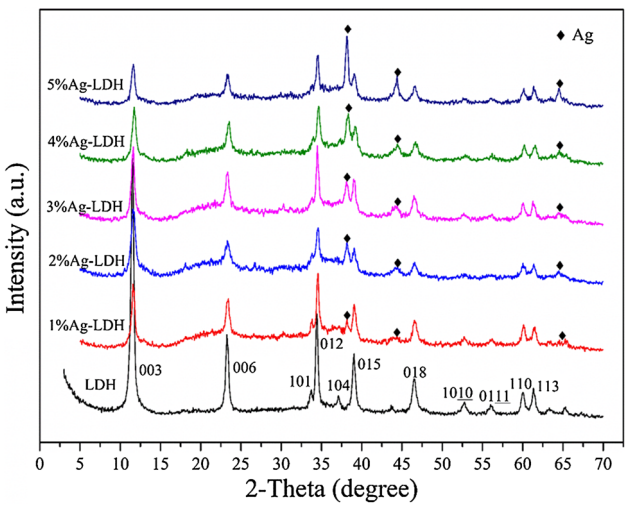

Figure 2 XRD patterns of the as-prepared LDH and *n*Ag/LDH composites (*n* = 1, 2, 3, 4 and 5%).

The optical properties

The UV–Vis of LDH and various Ag/LDH composites are shown in Fig. 4. It can be seen that the pure LDH showed an excellent absorption in ultraviolet region, with a clear absorption edge at around 350 nm. In contrast, with the addition of Ag, the absorption became much stronger in the visible range attributed to the SPR of Ag nanoparticles [41]. Furthermore, 4%Ag/LDH exhibited the highest absorption intensity, while the absorption intensity of 5%Ag/LDH decreased slightly. This could be

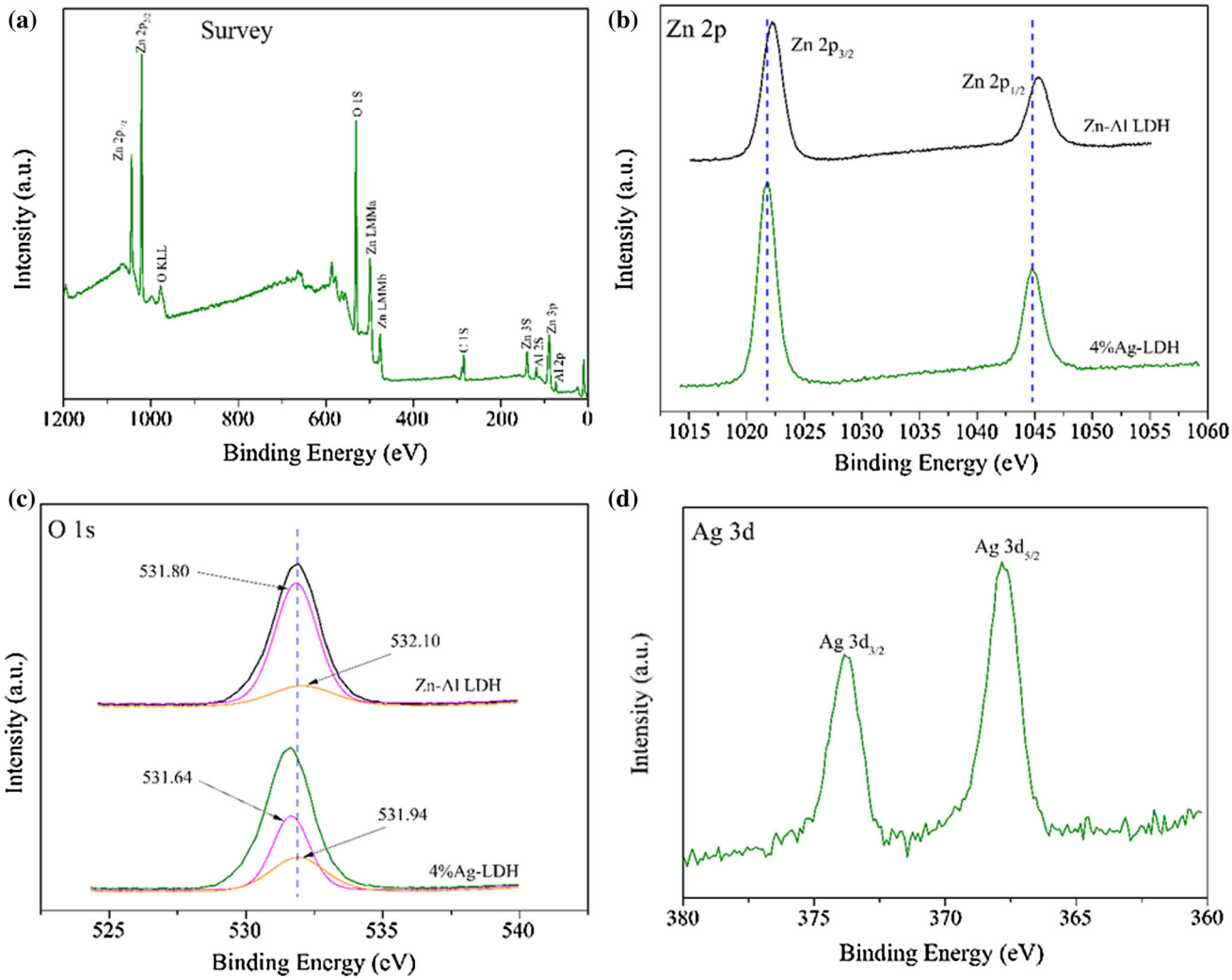

Figure 3 XPS spectra of 4%Ag/LDH: **a** survey spectra, **b** Zn 2*p*, **c** O1*s* and **d** Ag 3*d* core-levels.

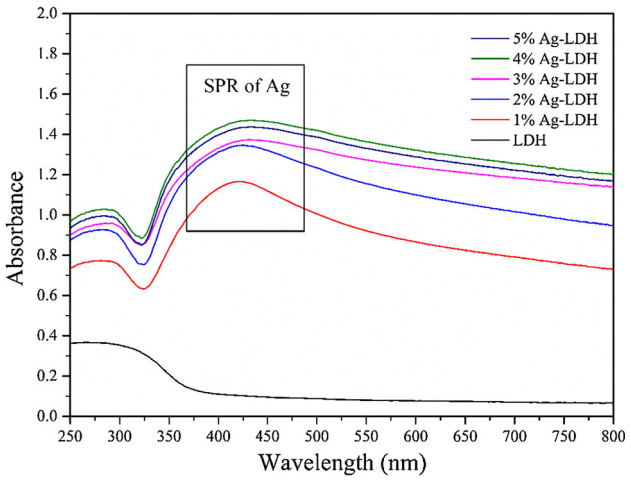

Figure 4 UV–Vis diffuse reflectance spectra of Ag/LDH with various Ag contents.

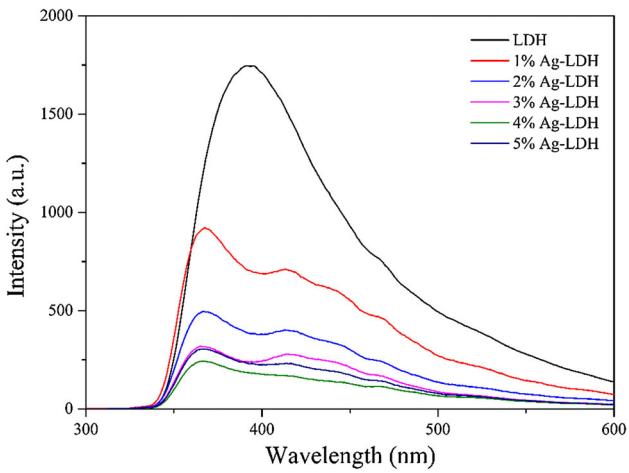

Figure 5 Photoluminescence spectra of LDH and Ag/LDH composites.

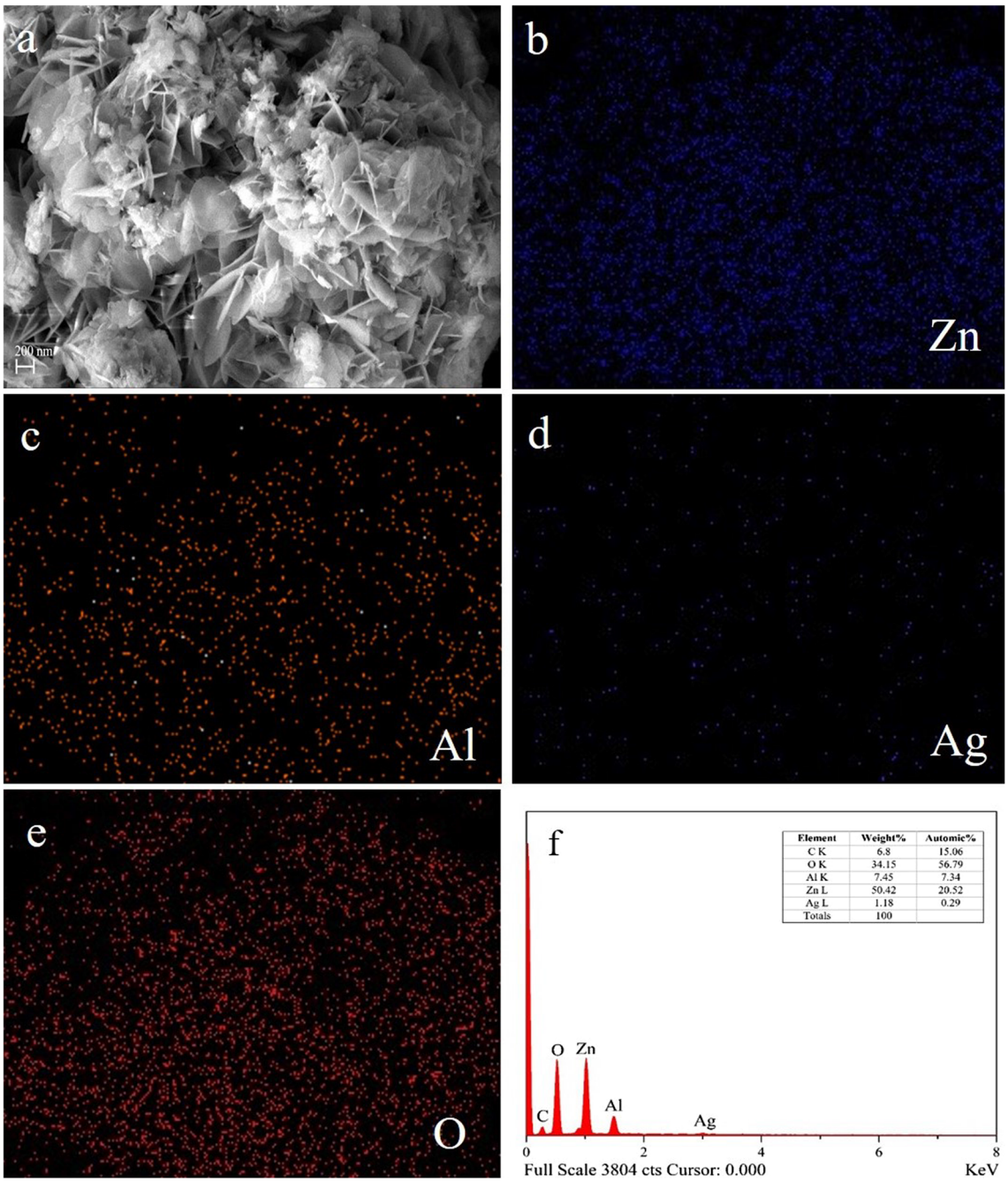

Figure 6 SEM image (**a**), EDS elemental map for the Zn (**b**), Al (**c**), Ag (**d**), O (**e**) and EDS spectra (**f**) of 4%Ag/LDH composite.

attributed to the larger cluster formed by Ag nanoparticles on the surface of LDH at higher Ag dosage, which was consistent with previous studies [23, 42]. The band-gap energy (E_g) was calculated by the Tauc relation using data of optical absorption versus wavelength near the band edge according to following equation [13]:

$$\alpha h\nu = A\left(h\nu - E_g\right)^n \quad (2)$$

where h was Planck's constant, ν was the frequency of vibration, A was a constant, E_g was the value of band-gap, α was the absorption coefficient, n decided the characteristics of the transition in a semiconductor. For allowed direct transition with $n = 1/2$ [43], in this case, the energy band-gap calculated for pure Zn–Al LDH was 3.1 eV, which was well consistent with previous reported results [44].

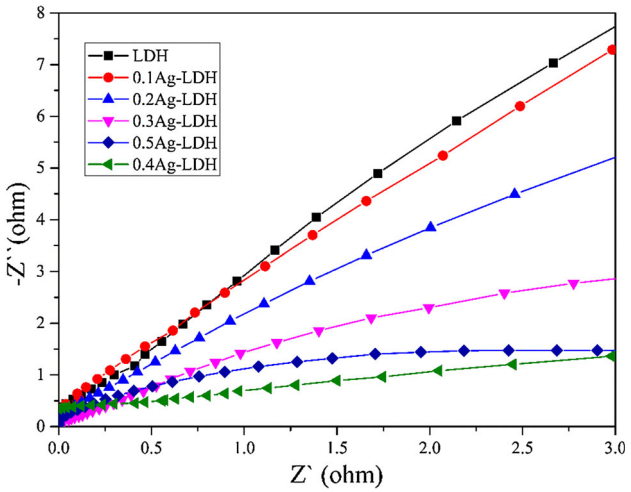

Figure 7 EIS Nyquist plots of pure Zn–Al LDH and Ag/LDH composites.

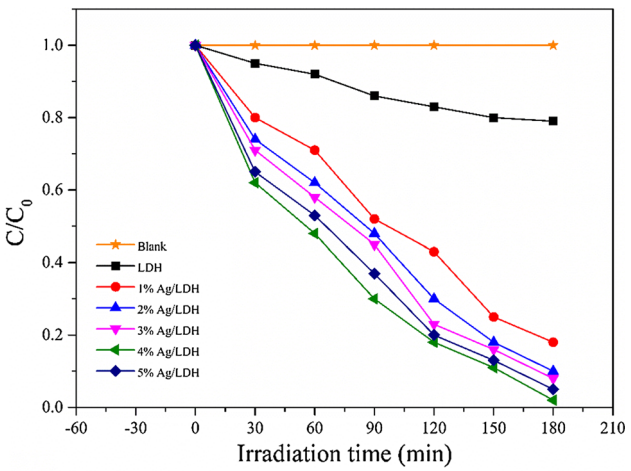

Figure 8 Photocatalytic degradation of MO using LDH and Ag/LDH composites as photocatalysts.

Photoluminescence spectroscopic (PL) analysis was used to study the recombination of electrons and holes in Ag/LDH composites, and the results are shown in Fig. 5. Compared with pure LDH, the Ag/LDH compounds with different Ag ratio showed lower emission intensity, indicating that the recombination of the photogenerated hole-electron pairs was obviously suppressed after the Ag loading on the surface of LDH, resulting from the efficient charge transfer between Ag and LDH matrix due to the Schottky barriers, consistent with the XPS results. Notably, the emission intensity first decreased and then increased with the increase in the dosage of Ag. Obviously, 4%Ag/LDH showed the lowest emission intensity as the optimized SPR effect of Ag nanoparticles on the surface of LDH. When overloaded, Ag nanoparticles would adversely work as recombination centers, therefore reducing the suppression ability and photocatalytic efficiency [29, 45].

Morphologic characterization

Since the 4%Ag/LDH sample exhibited the best optical properties, it was chosen for morphologic characterization. As shown in Fig. 6, there was a strong tendency for the cluster formation during all grinding process. The SEM image clearly confirmed the presence of typical laminar flocculation of LDH. Simultaneously, some tiny particles could be observed on the surface of LDH, which could be attributed to Ag nanoparticles. In other words, the presence of Ag did not destroy the typical layered structure of LDH. Ag could be directly loaded onto the surface of LDH to form a composite through mechanochemical operation. The EDS mapping was selected for further analysis of elemental distribution on composite. Zn, Al, C, O and Ag elements of 4%Ag/LDH were well distributed on the surface of composite, which could prove the uniform dispersion of Ag on the LDH matrix as nanoparticles. The chemical compositions of all elements were fitted near to the starting sample.

Photoelectrochemical performances

Since the photocatalytic capacity of the semiconductors depends mainly on the migration efficiency and recombination rate of photogenerated charge carriers, electrochemical impedance spectroscopy (EIS) test was carried out to further examine the electron transfer capacity and the electron–hole separation [46]. It is known that the arc radius on the EIS Nyquist plot reflects the reaction rate on the surface of the electrode. The separation efficiency of photogenerated electrons from holes is inversely proportional to the arc radius. The smaller the arc radius is, the higher the efficiency of charge migration across the electrode–electrolyte interface [47]. As shown in Fig. 7, the arc radius of Ag/LDH was much smaller than that of the pure LDH, due to the suppressed recombination of electron–hole pairs. Similarly, the arc radius of 4%Ag/LDH composite exhibited smallest value among the composites and excessive Ag nanoparticles would lead to the disturbance of recombination of electrons and holes. The curvatures

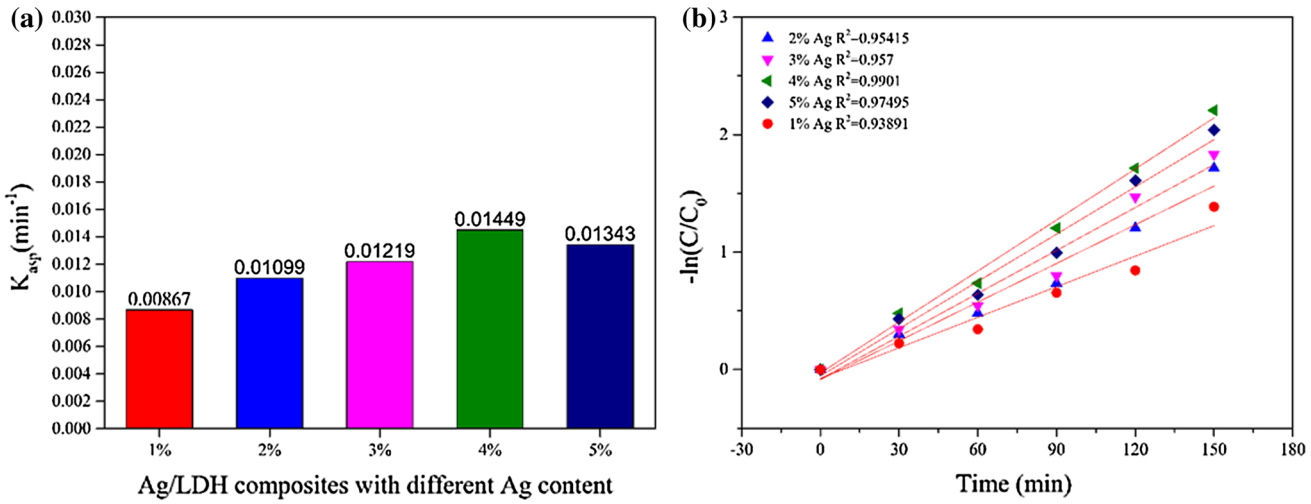

Figure 9 Apparent rate constants for the photocatalytic degradation of MO by Ag/LDH composites (**a**) and plots of the dependence of $-\ln(C/C_0)$ on irradiation time (**b**).

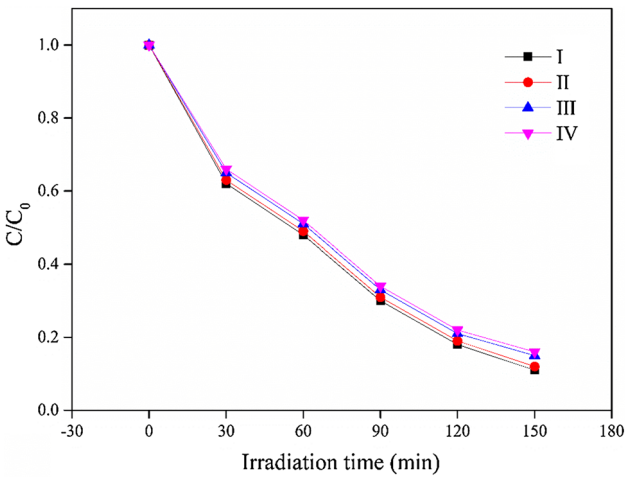

Figure 10 Photocatalytic stability tests showing C/C_0 for the 4%Ag/LDH photocatalysts after 4 (I–IV) reaction runs.

of EIS Nyquist plot curves were not particularly obvious because of the relative low crystallinity of mechanochemically synthesized materials. This phenomenon has also appeared in some other studies [48–50].

Photocatalytic activity

The photocatalytic performances on MO degradation by pure LDH and Ag/LDH under visible light irradiation are shown in Fig. 8. MO could be rarely degraded without photocatalysts under visible light, and the pure LDH exhibited weak photocatalytic activity due to the large energy gap (3.1 eV). After Ag loading, Ag/LDH composites could utilize the visible light because of the SPR effect and facilitated efficiently the degradation of MO. The 4%Ag/LDH showed the best photoactivity, degrading MO in solution almost completely after 180 min. The optimal value of Ag particles loading could absorb resonant photons and transfer electrons to the conduction band of LDH which could facilitate the separation of e^- and h^+. Insufficient Ag loading would not provide enough electrons to the CB of LDH, while overweight Ag could be the recombination center of photogenerated carriers.

Photodegradation kinetics of MO by various catalysts were usually described by the Langmuir–Hinshelwood model (Fig. 9). The photocatalytic process of MO was expressed as the following apparent pseudo-first-order kinetics equation [51], where $k\alpha$ is the apparent pseudo-first order rate constant (min^{-1}), C is the concentration of MO (mg/L) in aqueous solution at t min, C_0 is the initial concentration of MO. The apparent rate constants were determined from the regression curves of $-\ln(C/C_0)$ versus irradiation time, in which the value of rate constant k_{asp} was equal to the corresponding slope of the fitting line. The highest value of k_{asp} was 0.01449 min^{-1} of 4%Ag/LDH, which further proved that the loading of appropriate amount of Ag on LDH matrix could significantly increase the photocatalytic activity of MO. There existed an optimal value for silver usage.

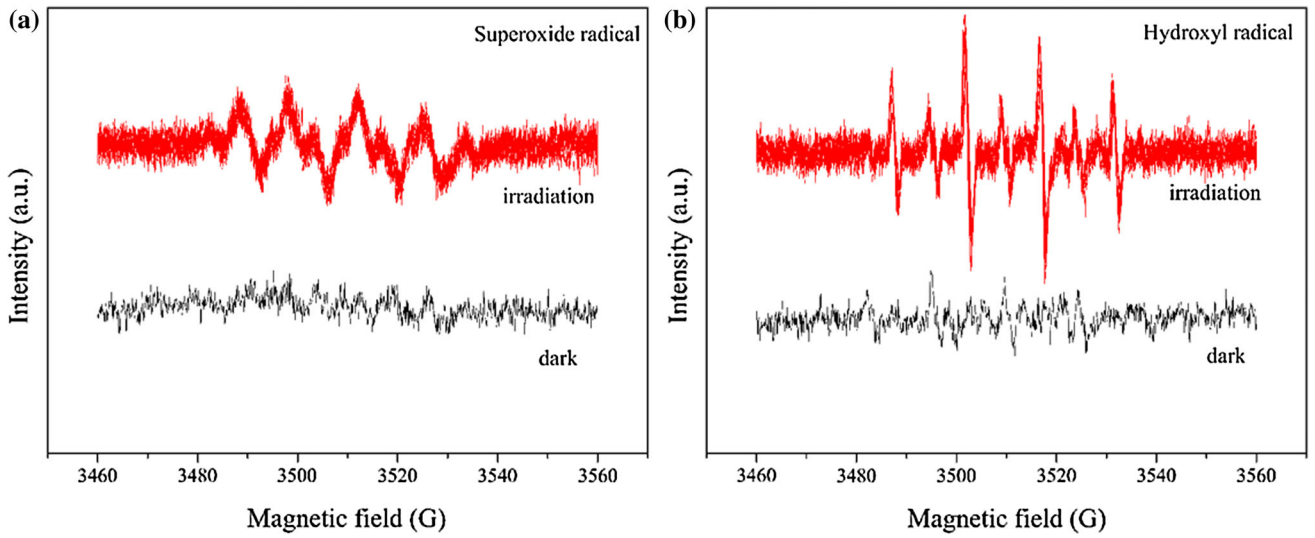

Figure 11 DMPO spin-trapping ESR spectra for 4%Ag/LDH in aqueous dispersion for DMPO-·OH and in methanol dispersion for DMPO-·O^{2-}.

Figure 12 Photocatalytic degradation mechanism of Ag/Zn–Al LDH composite.

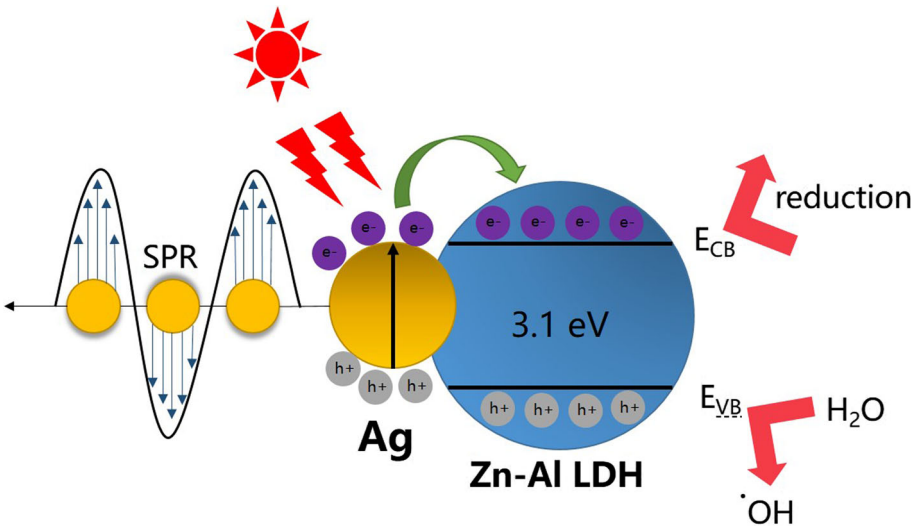

$$-\ln\frac{C}{C_0} = k_{asp}t \tag{3}$$

$$t_{\frac{1}{2}} = \frac{\ln 2}{k_{asp}} \tag{4}$$

To verify the stability and recyclability of Ag/LDH, the 4%Ag/LDH sample was used four times under visible light irradiation, as shown in Fig. 10. After each cycle, the catalyst was collected by centrifugation and washed with high purity deionized water until a clear supernatant was obtained. The wash catalyst was dried without light irradiation and used again for the degradation of a freshly prepared MO solution. The photocatalyst showed a slight loss of activity after four cycles, which might mainly be attributed to the loss of the photocatalyst during the washing operation between the cycles.

Photocatalytic degradation mechanism

To further investigate the mechanism of the photogradation, the spin-trapping ESR measurement was used over the 4%Ag/LDH nanocomposites under illumination of visible light. Figure 11 shows the ESR spectra of both the hydroxyl radical and the superoxide radical. It was observed that the peak intensity of hydroxyl radical was much higher than that of superoxide radical, demonstrating that hydroxyl

radical was the main reactive species in the photocatalytic process.

The mechanism of photocatalytic degradation of MO by Ag/LDH and the transfer pathway of charge carriers are schematically illustrated in Fig. 12. Given the difference in the work function of metals and semiconductors, a Schottky barrier could be formed between Ag and LDH under visible light illumination. Ag nanoparticles absorbed the resonant photons and the photogenerated electrons transferred from Ag to LDH until the two levels reached equilibrium to form a new Fermi energy level [52]. Under visible light irradiation, Ag/LDH was excited to form e^-–h^+ pairs over silver due to SPR of Ag. These photogenerated electrons were quickly transferred to the CB of LDH and left holes on VB. These electrons and the hydroxyl radicals from the oxidization of H_2O by h^+ can effectively degrade organics to H_2O and CO_2. On the other hand, the SPR effect of spatially confined electrons in the deposited Ag nanoparticles propelled the Ag/LDH to absorb more visible light [41].

Conclusion

In this study, a series of plasmonic Ag loaded Zn–Al LDH nanoparticles have been synthesized successfully through mechanochemical operation. Ag nanoparticles were distributed uniformly on the surface of LDH even with element Ag rather than soluble salt as starting sample. The as-synthesized semiconductor materials were confirmed to exhibit significant photodegradation activity on MO under visible light, and 4%Ag/LDH composite exhibited the highest photocatalytic activity. This work provided a novel and environment-friendly means to fabricate a series of Ag loaded photocatalysts with efficient visible light response.

Compliance with ethical standards

Conflict of interest The authors declare that they have no conflict of interest.

References

[1] Mittal A, Mittal J, Malviya A, Kaur D, Gupta VK (2010) Decoloration treatment of a hazardous triarylmethane dye, light green SF (yellowish) by waste material adsorbents. J Colloid Interface Sci 342(2):518–527. https://doi.org/10.1016/j.jcis.2009.10.046

[2] Mittal A, Mittal J, Malviya A, Gupta VK (2009) Adsorption removal of hazardous anionic dye "Congo red" from wastewater using waste materials and recovery by desorption. J Colloid Interface Sci 340:16–26. https://doi.org/10.1016/j.jcis.2009.08.019

[3] Forgacs E, Cserhati T, Oros G (2004) Removal of synthetic dyes from wastewaters: a review. Environ Int 30(7):953–971. https://doi.org/10.1016/j.envint.2004.02.001

[4] Chong MN, Jin B, Chow CW, Saint C (2010) Recent developments in photocatalytic water treatment technology: a review. Water Res 44(10):2997–3027. https://doi.org/10.1016/j.watres.2010.02.039

[5] Zhao J, Yang X (2003) Photocatalytic oxidation for indoor air purification: a literature review. Build Environ 38(5):645–654. https://doi.org/10.1016/s0360-1323(02)00212-3

[6] Wang J, Yang Z, Gao X et al (2017) Core-shell g-C_3N_4@-ZnO composites as photoanodes with double synergistic effects for enhanced visible-light photoelectrocatalytic activities. Appl Catal B Environ 217:169–180. https://doi.org/10.1016/j.apcatb.2017.05.034

[7] Hao Q, Wang R, Lu H et al (2017) One-pot synthesis of C/Bi/Bi_2O_3 composite with enhanced photocatalytic activity. Appl Catal B 219:63–72. https://doi.org/10.1016/j.apcatb.2017.07.030

[8] Xia S-J, Liu F-X, Ni Z-M, Shi W, Xue J-L, Qian P-P (2014) Ti-based layered double hydroxides: efficient photocatalysts for azo dyes degradation under visible light. Appl Catal B Environ 144:570–579. https://doi.org/10.1016/j.apcatb.2013.07.060

[9] Cross HE, Parkes G, Brown DR (2012) Microwave calcination of Cu/Mg/Al hydrotalcite catalyst precursor. Appl Catal A Gen 429–430:24–30. https://doi.org/10.1016/j.apcata.2012.03.046

[10] Baliarsingh N, Parida KM, Pradhan GC (2014) Effects of Co, Ni, Cu, and Zn on photophysical and photocatalytic properties of carbonate intercalated MII/Cr LDHs for enhanced photodegradation of methyl orange. Ind Eng Chem Res 53(10):3834–3841. https://doi.org/10.1021/ie403769b

[11] Cao Y, Wittert G, Taylor A, Adams R, Shi Z (2016) Associations between macronutrient intake and obstructive sleep apnoea as well as self-reported sleep symptoms: results from a cohort of community dwelling Australian Men. Nutrients 8(4):207. https://doi.org/10.3390/nu8040207

[12] Chen G, Qian S, Tu X et al (2014) Enhancement photocatalytic degradation of rhodamine B on nano Pt intercalated Zn–Ti layered double hydroxides. Appl Surf Sci 293:345–351. https://doi.org/10.1016/j.apsusc.2013.12.165

[13] Ls SS, Mehedi R, Malmivirta M et al (2016) Heteronuclear nanoparticles supported hydrotalcites containing Ni(II) and Fe(III) stable photocatalysts for Orange II degradation. Appl Clay Sci 132–133:641–649. https://doi.org/10.1016/j.clay.2016.08.016

[14] Mohapatra L, Parida KM (2012) Zn–Cr layered double hydroxide: visible light responsive photocatalyst for photocatalytic degradation of organic pollutants. Sep Purif Technol 91:73–80. https://doi.org/10.1016/j.seppur.2011.10.028

[15] Tian L, Zhao Y, He S, Wei M, Duan X (2012) Immobilized Cu–Cr layered double hydroxide films with visible-light responsive photocatalysis for organic pollutants. Chem Eng J 184:261–267. https://doi.org/10.1016/j.cej.2012.01.070

[16] Starukh G (2017) Photocatalytically enhanced cationic dye removal with Zn–Al layered double hydroxides. Nanoscale Res Lett 12:391. https://doi.org/10.1186/s11671-017-2173-y

[17] Abderrazek K, Najoua FS, Srasra E (2016) Synthesis and characterization of [Zn–Al] LDH: study of effect of calcination on the photocatalytic activity. Appl Clay Sci 119:229–235. https://doi.org/10.1016/j.clay.2015.10.014

[18] Seftel EM, Popovici E, Mertens M et al (2008) Zn-Al layered double hydroxides: synthesis, characterization and photocatalytic application. Microporous Mesoporous Mater 113:296–304. https://doi.org/10.1016/j.micromeso.2007.11.029

[19] Li B, Zhao Y, Zhang S, Gao W, Wei M (2013) Visible-light-responsive photocatalysts toward water oxidation based on NiTi-layered double hydroxide/reduced graphene oxide composite materials. ACS Appl Mater Interfaces 5(20):10233–10239. https://doi.org/10.1021/am402995d

[20] Bumajdad A, Madkour M (2014) Understanding the superior photocatalytic activity of noble metals modified titania under UV and visible light irradiation. Phys Chem Chem Phys 16(16):7146–7158. https://doi.org/10.1039/c3cp54411g

[21] Alammar T, Mudring A-V (2009) Facile preparation of Ag/ZnO nanoparticles via photoreduction. J Mater Sci 44(2):3218–3222. https://doi.org/10.1007/s10853-009-3429-4

[22] She P, Xu K, He Q, Zeng S, Sun H, Liu Z (2016) Controlled preparation and visible light photocatalytic activities of corn cob-like Au–ZnO nanorods. J Mater Sci 52(6):3478–3489. https://doi.org/10.1007/s10853-016-0639-4

[23] Samanta S, Martha S, Parida K (2014) Facile synthesis of Au/g-C_3N_4 nanocomposites: an inorganic/organic hybrid plasmonic photocatalyst with enhanced hydrogen gas evolution under visible-light irradiation. ChemCatChem 6(5):1453–1462. https://doi.org/10.1002/cctc.201300949

[24] Tang D, Zhang G (2017) Ultrasonic-assistant fabrication of cocoon-like Ag/$AgFeO_2$ nanocatalyst with excellent plasmon enhanced visible-light photocatalytic activity. Ultrason Sonochem 37:208–215. https://doi.org/10.1016/j.ultsonch.2017.01.010

[25] Chen H, Shao L, Li Q, Wang J (2013) Gold nanorods and their plasmonic properties. Chem Soc Rev 42(7):2679–2724. https://doi.org/10.1039/c2cs35367a

[26] Huang X, Neretina S, El-Sayed MA (2009) Gold nanorods: from synthesis and properties to biological and biomedical applications. Adv Mater 21(48):4880–4910. https://doi.org/10.1002/adma.200802789

[27] Li XZ, Li FB (2001) Study of Au/Au^{3+}–TiO_2 photocatalysts toward visible photooxidation for water and wastewater treatment. Environ Sci Technol 35(11):2381–2387. https://doi.org/10.1021/es001752w

[28] Wang Z, Zhao S, Zhu S, Sun Y, Fang M (2011) Photocatalytic synthesis of M/Cu_2O (M = Ag, Au) heterogeneous nanocrystals and their photocatalytic properties. CrystEngComm 13(7):2262–2267. https://doi.org/10.1039/c0ce00681e

[29] Liu H, Sun Q, Wang B, Wang P, Zou J (2016) Morphology and composition of microspheres in fly ash from the Luohuang Power Plant, Chongqing, Southwestern China. Miner Basel 6(2):30. https://doi.org/10.3390/min6020030

[30] Baláž M, Daneu N, Balážová Ľ, Dutková E, Tkáčiková Ľ, Briančin J, Vargová M, Balážová M, Zorkovská A, Baláž P (2017) Bio-mechanochemical synthesis of silver nanoparticles with antibacterial activity. Adv Powder Technol 28(12):3307–3312. https://doi.org/10.1016/j.apt.2017.09.028

[31] Apalangya V, Rangari V, Tiimob B, Jeelani S, Samuel T (2014) Development of antimicrobial water filtration hybrid material from bio source calcium carbonate and silver nanoparticles. Appl Surf Sci 295:108–114. https://doi.org/10.1016/j.apsusc.2014.01.012

[32] Li Z, Chen M, Zhang Q, Qu J, Ai Z, Li Y (2017) Mechanochemical synthesis of ultrafine ZnS/Zn–Al layered double hydroxide heterojunction and their photocatalytic activities in dye degradation. Appl Clay Sci 144:115–120. https://doi.org/10.1016/j.clay.2017.05.015

[33] Li Z, Zhang Q, He X, Chen M (2018) Enhanced visible light photocatalytic activity of the mechanochemically prepared nanosized $Zn_xCd_{1-x}S$/Zn–Al layered double hydroxide precursor heterojunctions. Appl Clay Sci 151:201–210. https://doi.org/10.1016/j.clay.2017.10.012

[34] Tongamp W, Zhang Q, Saito F (2007) Preparation of meixnerite (Mg–Al–OH) type layered double hydroxide by a mechanochemical route. J Mater Sci 42:9210–9215. https://doi.org/10.1007/s10853-007-1866-5

[35] Wang B, Qu J, Li X, He X, Zhang Q (2016) Precursor preparation to promote the adsorption of Mg–Al layered

double hydroxide. J Am Ceram Soc 99(9):2882–2885. https://doi.org/10.1111/jace.14404

[36] Chen C, Zheng Y, Zhan Y, Lin X, Zheng Q, Wei K (2011) Enhanced Raman scattering and photocatalytic activity of Ag/ZnO heterojunction nanocrystals. Dalton T 40(37):9566–9570. https://doi.org/10.1039/c1dt10799b

[37] Mou H, Song C, Zhou Y, Zhang B, Wang D (2018) Design and synthesis of porous Ag/ZnO nanosheets assemblies as super photocatalysts for enhanced visible-light degradation of 4-nitrophenol and hydrogen evolution. Appl Cataly B Environ 221:565–573. https://doi.org/10.1016/j.apcatb.2017.09.061

[38] Yi J, Song J, Mo H, Yang Y (2018) One step pyridine-assisted synthesis of visible-light-driven photocatalyst Ag/$AgVO_3$. Adv Powder Technol 29(2):319–324. https://doi.org/10.1016/j.apt.2017.11.018

[39] Hadnadjev-Kostic M, Vulic T, Marinkovic-Neducin R et al (2017) Photo-induced properties of photocatalysts: a study on the modified structural, optical and textural properties of TiO_2–ZnAl layered double hydroxide based materials. J Clean Prod 164:1–18. https://doi.org/10.1016/j.jclepro.2017.06.091

[40] Gu C, Cheng C, Huang H, Wong T, Wang N, Zhang T-Y (2009) Growth and photocatalytic activity of dendrite-like ZnO@Ag heterostructure nanocrystals. Cryst Growth Des 9(7):3278–3285. https://doi.org/10.1021/cg900043k

[41] Seery MK, George R, Floris P, Pillai SC (2007) Silver doped titanium dioxide nanomaterials for enhanced visible light photocatalysis. J Photochem Photobiol A 189:258–263. https://doi.org/10.1016/j.jphotochem.2007.02.010

[42] Zhang Y, Zhou J, Li Z, Feng Q (2017) Photodegradation pathway of rhodamine B with novel Au nanorods@ZnO microspheres driven by visible light irradiation. J Mater Sci 53(5):3149–3162. https://doi.org/10.1007/s10853-017-1779-x

[43] Xia SJ, Liu FX, Ni ZM, Xue JL, Qian PP (2013) Layered double hydroxides as efficient photocatalysts for visible-light degradation of Rhodamine B. J Colloid Interfaces Sci 405:195–200. https://doi.org/10.1016/j.jcis.2013.05.064

[44] Li H, Deng Q, Liu J et al (2014) Synthesis, characterization and enhanced visible light photocatalytic activity of Bi_2MoO_6/Zn–Al layered double hydroxide hierarchical heterostructures. Catal Sci Technol 4(4):1028–1037. https://doi.org/10.1039/c3cy00940h

[45] Xu T, Zhu R, Zhu J et al (2016) Fullerene modification of Ag_3PO_4 for the visible-light-driven degradation of acid red 18. RSC Adv 6(89):85962–85969. https://doi.org/10.1039/c6ra18657b

[46] Deng Q, Tang H, Liu G et al (2015) The fabrication and photocatalytic performances of flower-like Ag nanoparticles/ZnO nanosheets-assembled microspheres. Appl Surf Sci 331:50–57. https://doi.org/10.1016/j.apsusc.2014.12.202

[47] Zhang L, Li L, Sun X, Liu P, Yang D, Zhao X (2016) ZnO-layered double hydroxide@graphitic carbon nitride composite for consecutive adsorption and photodegradation of dyes under UV and visible lights. Materials 9:927. https://doi.org/10.3390/ma9110927

[48] Dong S, Ding X, Guo T, Yue X, Han X, Sun J (2017) Self-assembled hollow sphere shaped Bi_2WO_6/RGO composites for efficient sunlight-driven photocatalytic degradation of organic pollutants. Chem Eng J 316:778–789. https://doi.org/10.1016/j.cej.2017.02.017

[49] Liu G, You S, Huang H, Ma M, Ren N (2017) A novel Z-scheme $BiPO_4$–$Bi_2O_2(OH)(NO_3)$ heterojunction structured hybrid for synergistic photocatalysis. Chemosphere 171:702–709. https://doi.org/10.1016/j.chemosphere.2016.12.102

[50] Liu Y, Yao W, Liu D et al (2015) Enhancement of visible light mineralization ability and photocatalytic activity of $BiPO_4$/BiOI. Appl Catal B Environ 163:547–553. https://doi.org/10.1016/j.apcatb.2014.08.039

[51] Li S, Hu S, Jiang W, Liu Y, Liu J, Wang Z (2017) Facile synthesis of flower-like Ag_3VO_4/Bi_2WO_6 heterojunction with enhanced visible-light photocatalytic activity. J Colloid Interface Sci 501:156–163. https://doi.org/10.1016/j.jcis.2017.04.057

[52] Rajesh K, Santhanalakshmi J (2018) Fabrication of a SnO_2-graphene nanocomposite based electrode for sensitive monitoring of an anti-tuberculosis agent in human fluids. New J Chem 42(4):2903–2915. https://doi.org/10.1039/C7NJ03411C